

NEOROCKS project: surface properties of small near-Earth asteroids

T. Hromakina,^{1,2*} M. Birlan,^{3,4} M. A. Barucci,¹ M. Fulchignoni,¹ F. Colas,³ S. Fornasier,^{1,5} F. Merlin,¹ A. Sonka,⁴ S. Anghel,^{3,4,6} G. Poggiali,¹ I. Belskaya,^{1,2} D. Perna⁷ E. Dotto⁷ and the NEOROCKS team †

¹LESIA, Université Paris Cité, Observatoire de Paris, Université PSL, Sorbonne Université, CNRS, F-92190 MEUDON, France

²V. N. Karazin Kharkiv National University, 4 Svobody Sq., Kharkiv, 61022, Ukraine

³IMCCE, Observatoire de Paris, CNRS UMRO 8028, PSL Research University, 77 av Denfert Rochereau, 75014, Paris Cedex, France

⁴Astronomical Institute of the Romanian Academy, 5 Cutitul de Argint, 040557, sector 4, Bucharest, Romania

⁵Institut Universitaire de France (IUF), 1 rue Descartes, 75231 PARIS CEDEX 05

⁶Faculty of Physics, University of Bucharest, 405, Atomistilor Street, 077125 Magurele, Ilfov, Romania

⁷INAF – Osservatorio Astronomico di Roma, Via Frascati 33, 00078 Monte Porzio Catone, Italy

Accepted XXX. Received YYY; in original form ZZZ

ABSTRACT

We present new results of the observing program which is a part of the NEOROCKS project aimed to improve knowledge on physical properties of near-Earth Objects (NEOs) for planetary defense. Photometric observations were performed using the 1.2m telescope at the Haute-Provence observatory (France) in the BVRI filters of the Johnson-Cousins photometric systems between June 2021 and April 2022. We obtained new surface colors for 42 NEOs. Based on the measured colors we classified 20 objects as S-complex, 9 as C-complex, 9 as X-complex, 2 as D-type, one object as V-type, and one object remained unclassified. For all the observed objects we estimated their absolute magnitudes and diameters. Combining these new observations with the previously acquired data within the NEOROCKS project extended our dataset to 93 objects. The majority of objects in the dataset with diameters $D < 500\text{m}$ belongs to a group of silicate bodies, which could be related to observational bias. Based on MOID and ΔV values we selected 14 objects that could be accessible by a spacecraft. Notably, we find D-type asteroid (163014) 2001 UA5 and A-type asteroid 2017 SE19 to be of particular interest as possible space mission targets.

Key words: Minor planets, asteroids: general – Techniques: photometric – Surveys

1 INTRODUCTION

A population of near-Earth objects (NEOs) is believed to be brought into their current location from the asteroid belt due to the Yarkovsky effect and gravitational interactions with Jupiter and Saturn and defined by perihelion distance $q < 1.3$ au (Granvik et al. 2017; Bottke et al. 2006; Wisdom 1983). Such proximity to our planet gives us a chance to study these asteroids down to several meters in diameter, whereas main belt asteroids could be reached only down to hundreds of meters by the means of ground-based observations. Investigation of NEOs provides us with an opportunity to better understand the evolution of the solar system and the processes that took place at the early stages of its formation. Notably, NEOs are also a threat to

humanity due to potential collision hazard (e.g., Perna et al. 2013, 2016). In particular, NEOs with minimum orbital intersection distance $\text{MOID} < 0.05$ au and absolute magnitude $H < 22$ are classified as potentially hazardous asteroids (PHAs).

The number of discovered NEOs is constantly growing, but the number of NEOs with known physical properties is very small. According to the Light Curve Database (Warner et al. 2009, updated 14 December, 2021), rotational period and/or surface color is known for 2117 objects, which is only about 7% of the discovered NEOs. In addition, the majority of these objects are large NEOs. The rate at which new NEOs are being discovered only increases this gap. Thus, there is a need for dedicated surveys that would focus on investigating the physical properties of NEOs, particularly the smallest members of the population.

The whole variety of compositional classes is found among NEOs, with majority of the population (from 40 to 70%) represented by silicate S-complex asteroids (Devogèle et al. 2019; Ieva et al. 2018, 2020; Lin et al. 2018; Binzel et al. 2019; Popescu et al. 2019; Perna et al. 2018). However, the recent work by Marsset et al. (2022) that presented a debiased distribution of NEOs suggests that the low-albedo carbonaceous asteroids might be underrepresented, and the amount of silicate and carbonaceous asteroids is nearly equal.

Here we present the results of new observations conducted within the framework of the NEOROCKS project, which aims to character-

* E-mail: tetiana.hromakina@obspm.fr

† The NEOROCKS team: E. Dotto, M. Banaszekiewicz, S. Banchi, M.A. Barucci, F. Bernardi, M. Birlan, B. Carry, A. Cellino, J. De Leon, M. Lazzarin, E. Mazzotta Epifani, A. Medavilla, J. Nomen Torres, D. Perna, E. Perozzi, P. Pravec, C. Snodgrass, C. Teodorescu, S. Anghel, A. Bertolucci, F. Calderini, F. Colas, A. Del Vigna, A. Dell’Oro, A. Di Cecco, L. Dimare, P. Fatka, S. Fornasier, E. Frattin, P. Frosini, M. Fulchignoni, R. Gabryszewski, M. Giardino, A. Giunta, T. Hromakina, J. Huntingford, S. Ieva, J.P. Kotlarz, F. La Forgia, J. Licandro, H. Medeiros, F. Merlin, F. Pinna, G. Polenta, M. Popescu, A. Rozek, P. Scheirich, A. Sergeev, A. Sonka, G.B. Valsecchi, P. Wajer, A. Zinzi.

ize small NEOs by obtaining their surface colors and classify them into taxonomic classes.

In Section 2 we describe the observations and main results. Section 3 presents taxonomic classification of the observed NEOs. We present the analysis and discuss the results in Section 4. Finally, the summary and conclusions of this work are presented in Section 5.

2 OBSERVATIONS AND RESULTS

New photometric data presented in this work were obtained during several observational runs between June 2021 and April 2022 using the 1.2m telescope at the Haute-Provence observatory (OHP), located in France. The telescope is equipped with a 2048×2048 Andor Ikon L 936 CCD camera that has a field-of-view of 13.1'×13.1'. A 2×2 binning that was applied throughout all observing runs gave a 0.77"/pxl scale.

The selection of the targets was similar to the previous work (Hromakina et al. 2021): we prioritised objects with higher absolute magnitude (i.e. smaller objects) and PHAs. Additionally, newly discovered NEOs were also added to the priority list, because the discovery apparition is followed by a small window when the object is available for characterisation (e.g., Galache et al. 2015).

Observations were obtained in B-V-R-I filters of the Johnson-Cousins photometric system. Each object was observed for about an hour, which, depending on the exposure time from 30 seconds to 3 minutes, resulted in 3-15 images in each filter. The images in each filter were taken sequentially in order to minimize possible magnitude variation due to the rotation of an object.

Data reduction was done following the same approach that was described in Hromakina et al. (2021), which includes bias subtraction and flat-field correction. The instrumental magnitudes were measured for the target and field stars using aperture photometry. Then, absolute calibration was done using magnitudes of field stars in the Pan-STARRS catalog. To transform star magnitudes from the Sloan photometric system of the Pan-STARRS1 catalog into the Johnson-Cousins system we used transformational equations presented in Kostov & Bonev (2018).

We observed 42 small NEOs, about a quarter of which are recently discovered objects. Five objects observed during the April 2022 run were observed as part of the Rapid Response Experiment (Perna et al., in preparation), which is another objective of the NEOROCS programme. Nearly 40% of the observed NEOs (16 out of 42) are classified as PHAs. Table 1 contains the photometry results, estimated absolute magnitudes and diameters, and observational circumstances of our data. The orbital elements of the observed asteroids are presented in Table A1 of the Appendix A.

Absolute magnitudes (H) given in Table 1 were calculated using our measurements of V magnitudes via the online tools for H, G_1, G_2 photometric system¹. It was shown that the one-parameter version of the H, G_1, G_2 function can give reliable results even in the case of only one magnitude measurement (Penttilä et al. 2016). We compared our absolute magnitudes with the values presented in the Minor Planetary Center (MPC) and found generally good agreement. For three asteroids 2010 WQ7, 2022 BQ3, and 2022 DC5 the discrepancies exceed 0.5 mag. Further observations are needed to find possible reasons for these discrepancies. Absolute magnitude distribution of the sample is shown in Fig. 1. Almost all of the observed NEOs

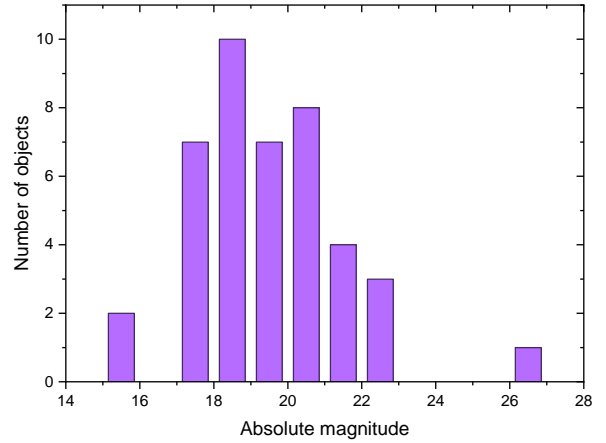


Figure 1. Absolute magnitude distribution of the observed NEOs.

fall into the 17-23 mag range, with the largest absolute magnitude reaching $H \sim 26$.

To estimate the diameters of the observed objects we used the obtained absolute magnitudes and albedos of the respective taxonomic classes from Ryan & Woodward (2010). For the unclassified object 2022 GY2 we assumed S-complex taxonomic class. For 4 out of 42 NEOs in our sample the diameters were measured by the NEOWISE survey (Mainzer et al. 2019). Our estimations are well-consistent with the measured values within the uncertainties. In Table 1 we provide the NEOWISE diameters for four asteroids.

Table 1 also contains the results of the taxonomic classification that was performed in this work and described in the next section.

3 TAXONOMY

Taxonomic classification was done using the obtained surface colors B-V, V-R, and V-I, which were transformed into reflectances using the following equation:

$$R(\lambda) = 10^{-0.4[(M_\lambda - M_V) - (M_\lambda - M_V)_\odot]}, \quad (1)$$

where $(M_\lambda - M_V)$ and $(M_\lambda - M_V)_\odot$ are the colors of the object and the Sun at the wavelength λ , respectively. Solar colors were taken from Holmberg et al. (2006). The obtained reflectance was normalized at the central wavelength of the V-filter. Then, using the M4AST service (Popescu et al. 2012; Birlan et al. 2016), the resulting spectra were compared to the mean spectra of the taxonomic classes in DeMeo classification (DeMeo et al. 2009). In the case when the object was observed for two nights the average surface colors were used for taxonomic classification. One asteroid from the dataset, 2022 GY2, was not classified because only V-R color was measured. As our taxonomic classification is based on only three or four data points, it is not nearly as precise as spectral data. Thus, in Table 1 we indicate the major taxonomic classes, such as S-complex, C-complex, X-complex, A-type, D-type, and V-type. However, in the case of an unambiguous match to a specific sub-type according to Bus-DeMeo classification, we indicate both the sub-type and the major type. Some asteroids in our sample revealed similarity with Q-type, first defined by (Tholen 1984) for a near-Earth asteroid and considered as an end member class in DeMeo et al. (2009). In our further analysis we consider Q-type as a part of the S-complex. Figure B1 in Appendix B shows individual reflectance spectra of asteroids together with the mean spectra of the best-matching taxonomic class.

¹ <https://wiki.helsinki.fi/display/PSR/HG1G2+tools>

Table 1. Observational circumstances and results.

Object	Date	r, au	Δ , au	α , deg	V mag	B-V	V-R	V-I	Taxon	H	D, m	
1	(12923) Zephyr	27/11/2021	1.408	0.618	37.1	17.21±0.02	0.94±0.04	0.45±0.03	0.70±0.04	Q/S	16.1	2060±10*
2	(87024) 2000 JS66	09/06/2021	1.063	0.166	69.1	17.72±0.02	0.71±0.02	0.37±0.02	0.83±0.04	X	19.0	670-1080
3	(89958) 2002 LY45	11/06/2021	1.305	0.362	31.9	16.94±0.02	0.75±0.04	0.47±0.02	0.75±0.02	Q/S	17.3	1100-1330
4	(138971) 2001 CB21	28/01/2022	1.165	0.251	39.6	17.43±0.03	0.92±0.04	0.39±0.03	0.82±0.04	X	18.4	940-1190
		29/01/2022	1.160	0.242	39.5	17.24±0.03	0.84±0.04	0.43±0.02	0.79±0.03			
5	(140158) 2001 SX169	09/06/2021	1.097	0.128	47.5	15.89±0.01	0.76±0.03	0.46±0.02	0.82±0.02	Xe/X	18.4	566±10*
6	(143649) 2003 QQ47	02/10/2021	1.068	0.173	63.1	16.12±0.02	0.90±0.03	0.52±0.02	0.86±0.02	S	17.5	950-1160
7	(162913) 2001 MT18	09/06/2021	1.017	0.206	83.8	18.06±0.02		0.55±0.02	1.05±0.03	D	18.5	940-1310
8	(163692) 2003 CY18	05/04/2022	1.307	0.355	26.7	18.03±0.02	0.84±0.03	0.49±0.02	0.94±0.03	S	18.5	630-760
9	(318160) 2004 QZ2	27/01/2022	1.389	0.407	5.7	17.46±0.02	0.81±0.02	0.47±0.02	0.77±0.03	Sq/S	18.2	690-840
10	(363027) 1998 ST27	01/10/2021	1.152	0.194	36.1	17.72±0.02	0.78±0.03	0.42±0.02	0.75±0.03	C	19.6	578±228*
		02/10/2021	1.146	0.192	37.5	17.78±0.02	0.73±0.02	0.39±0.02	0.72±0.03			
11	(363599) 2004 FG11	05/04/2022	1.082	0.102	35.7	17.57±0.02	0.76±0.02	0.43±0.02	0.74±0.02	Xe/X	21.2	152±3*
		06/04/2022	1.069	0.090	39.5	17.18±0.02	0.77±0.02	0.43±0.02	0.71±0.02			
12	(366746) 2004 LJ	10/06/2021	1.112	0.142	44.5	17.80±0.02		0.51±0.03	0.76±0.03	Sq/S	20.15	260-320
13	(374855) 2006 VQ13	26/11/2021	1.138	0.176	28.6	17.85±0.02	0.71±0.04	0.44±0.03	0.82±0.10	X	20.1	370-590
		27/11/2021	1.145	0.182	27.5	17.89±0.03		0.50±0.03	0.87±0.03			
14	(388945) 2008 TZ3	05/04/2022	1.185	0.203	22.6	18.33±0.03	0.73±0.03	0.41±0.03	0.68±0.04	Cg/C	20.3	370-480
15	(410195) 2007 RT147	28/01/2022	1.361	0.383	9.2	17.32±0.02	0.75±0.04	0.45±0.03	0.66±0.04	Q/S	18.2	580-700
16	(415029) 2011 UL21	10/06/2021	1.181	0.540	59.1	16.90±0.02	0.82±0.04	0.47±0.02	0.86±0.03	Q/S	15.7	1900-2310
		11/06/2021	1.191	0.542	58.2	16.90±0.02	0.78±0.04	0.49±0.02	0.88±0.03			
17	(450263) 2003 WD158	08/06/2021	1.007	0.072	94.6	16.91±0.02		0.52±0.03	0.90±0.04	S	19.4	460-550
		10/06/2021	1.014	0.066	89.1	16.77±0.02	0.84±0.03	0.48±0.02	0.86±0.03			
18	(475665) 2006 VY13	06/04/2022	1.338	0.456	35.3	17.72±0.02		0.35±0.03	0.65±0.03	C	17.4	1630-2070
19	(491567) 2012 RG3	10/06/2021	1.242	0.382	46.1	18.34±0.03		0.41±0.03	0.92±0.03	D	18.3	1030-1430
20	(495615) 2015 PQ291	09/06/2021	1.215	0.334	46.5	17.37±0.02	0.83±0.03	0.47±0.02	0.88±0.03	S	17.6	790-960
21	(506459) 2002 AL14	29/01/2022	1.127	0.152	19.8	15.10±0.01	0.88±0.02	0.50±0.02	0.92±0.02	S	18.0	760-920
22	(516396) 2000 WY28	26/11/2021	1.165	0.180	7.0	17.88±0.02	0.90±0.05	0.36±0.05	0.67±0.05	C	20.8	430-550
23	(613291) 2005 YX128	28/01/2022	1.072	0.176	56.0	17.35±0.02	0.80±0.03	0.42±0.02	0.72±0.03	C	18.9	710-910
24	(613403) 2006 GB	04/04/2022	1.056	0.107	55.8	17.39±0.02	0.77±0.02	0.40±0.02	0.77±0.03	C	20.1	390-500
25	2002 TP69	26/11/2021	1.041	0.057	17.7	16.81±0.01	0.84±0.03	0.50±0.02	0.93±0.02	S	22.0	120-150
		27/11/2021	1.043	0.059	16.3	16.85±0.02	0.87±0.03	0.51±0.02	0.92±0.02			
26	2009 CC3	05/04/2022	1.045	0.143	68.1	17.38±0.02	0.96±0.04	0.52±0.02	0.77±0.02	S	19.1	460-550
27	2010 TV149	04/04/2022	1.079	0.177	60.3	17.08±0.02	0.78±0.03	0.42±0.02	0.79±0.03	X	18.5	670-1080
28	2010 WQ7	28/01/2022	1.130	0.248	48.8	18.26±0.02	0.75±0.04	0.51±0.03	0.88±0.03	S/S	19.2	630-760
29	2011 YQ10	26/11/2021	1.308	0.324	6.9	17.83±0.02	0.72±0.02	0.49±0.02	0.63±0.02	Q/S	19.1	440-530
30	2017 UW42	27/01/2022	1.268	0.336	28.2	17.34±0.01	0.87±0.02	0.50±0.02	0.91±0.02	S	17.9	760-920
31	2018 CW13	28/01/2022	1.177	0.193	5.0	17.03±0.02	0.80±0.03	0.43±0.02	0.72±0.03	Cg/C	19.9	450-570
32	2021 JQ24	27/11/2021	1.378	0.420	18.0	17.53±0.02	0.67±0.03	0.40±0.02	0.73±0.03	Xe/X	17.8	1010-1630
33	2021 LN3	11/06/2021	1.103	0.093	19.2	17.22±0.02		0.46±0.03	0.73±0.05	Q/S	21.2	150-180
34	2021 SR41**	06/04/2022	1.144	0.275	52.5	19.14±0.03	0.82±0.03	0.39±0.03	0.72±0.03	C	19.7	470-600
35	2021 VM25**	08/04/2022	1.043	0.073	53.1	16.71±0.02	0.71±0.03	0.49±0.02	0.86±0.03	S	20.4	360-500
36	2021 WX3	04/04/2022	1.116	0.132	27.1	17.48±0.02	0.71±0.02	0.38±0.02	0.67±0.02	C	20.4	360-450
37	2022 BH3	29/01/2022	0.998	0.016	31.6	18.57±0.02	0.91±0.03	0.51±0.02		S	26.3	10-20
38	2022 BK	27/01/2022	1.037	0.057	23.4	17.66±0.02		0.43±0.02	0.82±0.03	X	22.7	110-170
39	2022 BQ3	05/04/2022	1.147	0.218	43.5	17.72±0.02	1.00±0.03	0.5±0.02	0.64±0.03	V	19.1	240-280
40	2022 DC5**	06/04/2022	1.039	0.068	53.6	18.62±0.02		0.43±0.02	0.70±0.03	X	22.4	80-90
41	2022 GC1**	04/04/2022	1.112	0.117	15.9	18.94±0.02		0.52±0.02	0.87±0.03	S	22.5	80-100
42	2022 GY2**	08/04/2022	1.051	0.059	31.8	17.04±0.03		0.38±0.03			21.8	120-190

* Measured by NEOWISE survey (Mainzer et al. 2019).

**These objects were observed as part of the Rapid Response Experiment (Perna et al., in preparation).

We checked our classification using color-color plots (Figure 2). Boxes in the figures represent 1σ deviation of silicate and carbonaceous objects (see sect. 4). Some of the asteroids in the color-color diagrams seem to be "outliers", so we looked more closely into these objects. Asteroid (162913) 2001 MT18 is classified as D-type and has very red surface colors. Taking into account that this NEO was observed at a large phase angle (83.8°), its very red colors may be a result of phase reddening (e.g., Schröder et al. 2014; Perna et al. 2018). Other S-complex "outliers" are classified as Q-types, fresh-surfaced asteroids with more neutral slopes compared to S-type asteroids.

One more way to establish the reliability of the taxonomic classification is to compare the obtained results for the objects that were already classified based on more informative spectral data. Only two objects in this work, namely (12923) Zephyr and (506459) 2002 AL14 were previously classified by using spectral data as S-complex and L-type, respectively (Binzel et al. 2004). And in this work both objects were classified into the S-complex class.

Additionally, geometric albedo values are available for four NEOs.

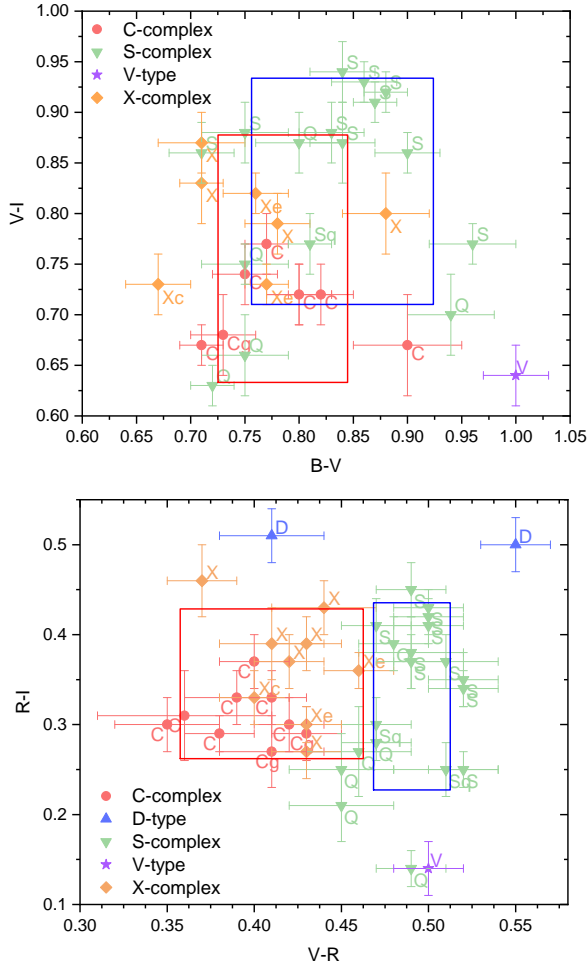
Among them, (12923) Zephyr, (140158) 2001 SX169, and (363599) 2004 FG11 that have moderate albedo compatible with the classification of these objects into S- and X-complexes. Similarly, NEO (363027) 1998 ST27 has a low albedo and is classified into C-complex in this work.

4 DATA ANALYSIS AND DISCUSSION

For the objects in our dataset, we calculated the average colors for each taxonomic class and compared them with those reported in the literature. Namely we use colors from DeMeo et al. (2009), that were derived from the spectral data, and colors from Ieva et al. (2018) and Lin et al. (2018), that were obtained from the broadband photometric observations (see Table 2). We found that the average colors obtained in this work are in general agreement with the literature values. We do not include A- and V-types in Table 2 as we have only a few asteroids classified into these taxons.

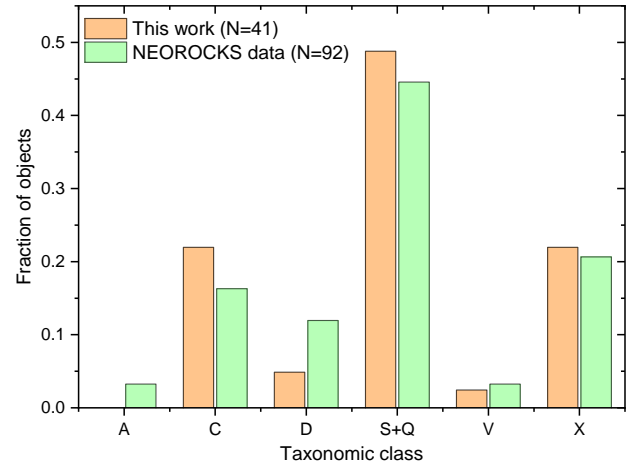
Table 2. Average colors obtained in this work for each taxonomic class in comparison to the literature values from DeMeo et al. (2009), Ieva et al. (2018), and Lin et al. (2018).

Taxonomic class	B-R	B-R <i>Lin18</i>	B-R <i>Ieva18</i>	B-R <i>DeMeo09</i>	V-I	V-I <i>Lin18</i>	V-I <i>Ieva18</i>	V-I <i>DeMeo09</i>
C	1.18±0.09	1.06	1.07±0.12	1.09±0.11	0.69±0.06	0.67	0.67±0.07	0.69±0.10
D	1.18±0.05	1.19	1.21±0.06	1.18±0.07	0.92±0.08	0.87	0.89±0.03	0.89±0.07
S	1.32±0.07	1.27	1.32±0.07	1.29±0.14	0.83±0.11	0.81	0.77±0.09	0.82±0.14
X	1.14±0.05	1.13	1.19±0.06	1.13±0.12	0.80±0.04	0.79	0.78±0.05	0.78±0.06

**Figure 2.** Color-color diagrams showing main taxonomic classes for our dataset. The boxes correspond to the 1σ deviation from the mean color values for the group of silicate (blue box) and carbonaceous (red box) objects.

For the new data the taxonomic classes are distributed as follows: 20 objects are classified as S-complex, both C- and X-complexes have 9 objects, 2 objects are D-type, and 1 object is classified as V-type. No objects were classified as A-type. By adding new surface color data for 42 NEOs, the NEOROCKS dataset increased to 93 objects. Considering the results obtained by Hromakina et al. (2021), in the extended sample of 92 objects (2022 GY2 not included) 46% are classified into S-complex, 18% into C-complex, 18% into X-complex, 13% as D-type, 3% as A-type, and 3% as V-type (Fig. 3).

Nearly a half of NEOs in our dataset fall into the S-complex. This predominance of silicate S-complex asteroids among NEOs is consistent with existing surveys on NEOs. Such prevalence of S-type asteroids among NEOs can be affected by an observational bias

**Figure 3.** Distribution of the taxonomic classes obtained in this work and the overall distribution for the NEOROCKS survey data.

towards objects with higher albedo. Thus, to obtain knowledge about the real compositional distribution, a debiasing technique should be applied. Given that the size of our sample is still relatively small, the debiasing of our data is beyond the scope of this work. We note that in the recent work by Marsset et al. (2022) the authors presented a debiased compositional distribution of NEOs. In particular, the portion of S-complex in their dataset drops from 66 to 42% for the bias-corrected distribution, and the amount of primitive C-complex asteroids doubles and goes from about 20 to about 40%.

As a significant portion of our data consists of PHAs, we looked for possible differences in the compositional distribution of PHAs and non-PHAs, and found no significant difference in the overall distribution between these two groups. The lack of compositional difference between PHAs and the rest of the NEOs population was also reported by Perna et al. (2016).

For further analysis, we split the classified objects in our dataset into groups of silicate objects, that includes S-complex, A-, and V-types, and carbonaceous objects, that consists of C-complex, D-type, and low-albedo X-types (also known as P-types in the Tholen taxonomy (Tholen 1984)). The remaining objects, namely X-complex asteroids with unknown albedo, are put into the miscellaneous group. This resulted in 47 objects in the silicate group, 28 objects in the carbonaceous group, and 17 objects in the miscellaneous group.

Figure 4 shows diameter distribution of the silicate, carbonaceous, and miscellaneous objects in the NEOROCKS dataset. The estimated sizes of the objects spread out from about 20 meters to almost 4 kilometers, with the majority of objects being in the $D < 1$ km range. The number of carbonaceous objects in our dataset steadily decreases with size. Silicate objects are much more prevalent among smaller objects, but its number drops significantly for $D > 1$ km. The relative ratio of carbonaceous to silicate objects with $D < 500$ m is 28% to

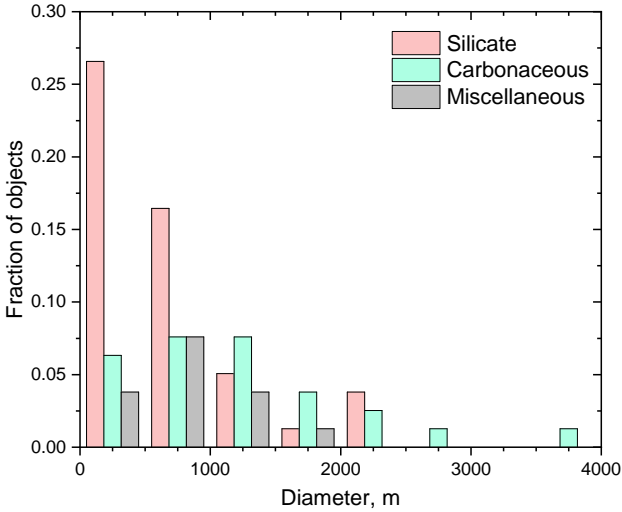


Figure 4. Size distribution of 92 NEOs in our dataset.

72%, and for objects with $D > 500$ m the ratio is 46 to 54%. Such distribution is most probably caused by the bias towards higher albedo objects.

We looked into the possible differences in the orbital and physical parameters between the different groups of objects analysed in this work. In Table 3 we present the median values of the main orbital elements, absolute magnitude, as well as the estimated diameter for the whole dataset, groups of silicate and carbonaceous objects, and also for the PHAs and non-PHAs. The "dispersion" of the median values was calculated as a median absolute deviation (MAD). Carbonaceous objects show slightly higher orbital inclinations and larger estimated diameters compared to the silicate ones. The Earth's MOID is lower for silicate objects, which in turn also suggests a generally lower MOID for smaller asteroids in our dataset because as we already established, the majority of objects with $D < 500$ m belong to the silicate group. PHAs in the dataset, as expected, have smaller q , Q , and a values, as well as slightly smaller diameters than non-PHAs. Otherwise, we do not find any significant correlations between the orbital and physical parameters for the objects in our dataset.

As already mentioned, close approaches of NEOs to Earth raise a concern due to the possible impact as well as create a possibility to investigate these objects *in situ* by a space mission. In this regard, objects with smaller Earth's MOIDs (i.e. PHAs) are better candidates for space mission targets. Another parameter that should be taken into consideration is ΔV , which is a measure of the impulse necessary for a spacecraft to reach the orbit of a target. According to Hinkle et al. (2015), with current propulsion technology, only objects with $\Delta V < 7$ km/s can be accessed by a spacecraft. Figure 5 shows Earth's MOID and ΔV values, that were taken from the MPC website, for the observed objects. In total, 14 objects have both $\text{MOID} < 0.05$ au and $\Delta V < 7$ km/s (Table 4). The majority of them (6 out of 10) belong to the silicate group, 3 objects are from the miscellaneous group and only one is from the carbonaceous group. Of particular interest are D-type and rare A-type asteroids, because they have not been visited by space missions yet (Barucci et al. 2018). In this regard, we can mention two objects from our data: D-type NEO (163014) 2001 UA5 and A-type NEO 2017 SE19. In Table 4 we also show the values of the parameter U, which corresponds to the orbit uncertainty, where 0 corresponds to a very small uncertainty and 9 indicates a very large uncertainty.

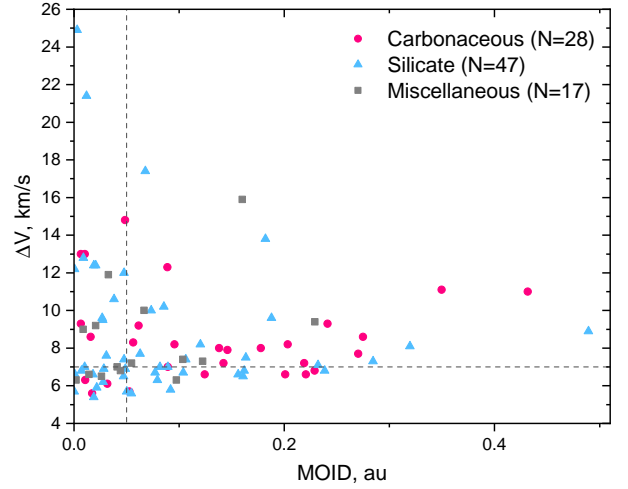


Figure 5. Earth's MOID vs. ΔV value for the NEOs in our dataset. Vertical and horizontal dashed lines at $\text{MOID} = 0.05$ au and $\Delta V = 7$ km/s, respectively, separate objects that may be suitable as space mission targets.

5 SUMMARY AND CONCLUSIONS

In this work we present new observational data for 42 small NEOs obtained within the NEOROCKS project. For these asteroids we computed surface colors, and estimated their taxonomic class, absolute magnitudes, and diameters. Based on the B-V, V-R, and V-I surface colors and considering only the main taxonomic classes, most of the observed objects (20 NEOs) were classified into the S-complex, 9 as C-complex, 9 as X-complex, 2 as D-type, and 1 as V-type.

By adding these new observational data we expanded our dataset to 93 objects. The compositional distribution of the updated dataset is as follows: most of the objects (46%) were classified into the S-complex, 18% into the X-complex, 18% into C-complex, and 13% as D-type. The remaining small number of objects were classified as A-types (3%) and V-types (3%). The calculated mean colors for the taxonomic classes considered in this work are in agreement with the literature values (DeMeo et al. 2009; Ieva et al. 2018; Lin et al. 2018). PHAs do not show a significant difference in the compositional distribution from the rest of the population.

Asteroids in our dataset with sizes $D < 500$ m predominantly belong to the silicate group. This result is due to the observational bias towards higher albedo objects rather than an intrinsic compositional difference.

The group of silicate objects shows lower Earth MOID compared to the group of low-albedo carbonaceous objects. Silicate objects also show a slightly smaller median inclination, but more data is needed to confirm a possible difference.

Finally, we selected objects that could be considered as space mission targets based on their MOID and ΔV values. Among 10 objects in our dataset that satisfy both criteria, we particularly note primitive D-type asteroids (163014) 2001 UA5 and rare A-type asteroid 2017 SE19.

The NEOROCKS project is still ongoing and new observational runs are scheduled. In the final article, which will be done at the end of the project, we will summarize the obtained results on the surface colors of NEOs and perform a global statistical analysis that will include available literature data.

Table 3. Median values of the orbital and physical parameters for the whole dataset and different sub-groups discussed in this work. The uncertainty value was calculated as median absolute deviation.

Group	e	i , deg	a , au	q , au	Q , au	MOID, au	H	D , m
All data (N=92)	0.49±0.08	10.38±6.24	1.78±0.50	0.94±0.19	2.74±0.83	0.06±0.05	19.00±1.15	572±290
PHAs (N=36)	0.50±0.09	9.92±6.61	1.58±0.50	0.78±0.18	2.39±0.89	0.02±0.01	19.30±1.10	540±268
non-PHAs (N=56)	0.49±0.06	11.38±6.50	2.12±0.49	1.03±0.15	3.12±0.83	0.12±0.06	18.85±1.15	666±263
Silicate (N=47)	0.48±0.04	11.38±7.42	1.95±0.39	0.95±0.14	2.93±0.71	0.05±0.03	19.00±1.10	495±305
Carbonaceous (N=28)	0.50±0.08	12.35±6.28	1.65±0.53	0.92±0.24	2.50±0.84	0.09±0.08	19.00±1.30	808±382
Miscellaneous (N=17)	0.54±0.09	9.79±4.63	1.69±0.60	0.97±0.23	2.71±1.13	0.05±0.04	18.7±1.10	603±269

Table 4. List of NEOs that could be potential space mission targets based on their low MOID and low ΔV .

Object	Taxon	ΔV , km/s	U*
(12923) Zephyr	S-complex	5.9	0
(52768) 1998 OR2	X-complex	6.6	0
(140158) 2001 SX169	X-complex	6.5	0
(332446) 2008 AF4	X-complex	6.3	0
(388945) 2008 TZ3	Cg/C-complex	5.6	0
(163014) 2001 UA5	D-type	6.1	0
(613403) 2006 GB	C-complex	6.4	0
2009 CC3	S-complex	6.9	0
2010 TV149	X-complex	6.8	0
2017 SE19	A-type	6.5	0
2002 TP69	S-complex	5.7	0
2020 RO6	S-complex	5.4	0
2020 YQ3	S-complex	6.8	0
2022 BH3	S-complex	6.6	6

*Orbit uncertainty parameter taken from the MPC website.

ACKNOWLEDGEMENTS

We acknowledge funding from the European Union's Horizon 2020 research and innovation programme under grant agreement No. 870403. The article is based on observations made at Observatoire de Haute Provence (CNRS), France.

DATA AVAILABILITY

The data underlying this article will be shared on reasonable request to the corresponding author.

REFERENCES

- Barucci M. A., et al., 2018, *MNRAS*, **476**, 4481
- Binzel R. P., Rivkin A. S., Stuart J. S., Harris A. W., Bus S. J., Burbine T. H., 2004, *Icarus*, **170**, 259
- Binzel R. P., et al., 2019, *Icarus*, **324**, 41
- Birlan M., Popescu M., Irimiea L., Binzel R., 2016, in AAS/Division for Planetary Sciences Meeting Abstracts #48, p. 325.17
- Botke William F. J., Vokrouhlický D., Rubincam D. P., Nesvorný D., 2006, *Annual Review of Earth and Planetary Sciences*, **34**, 157
- DeMeo F. E., Binzel R. P., Slivan S. M., Bus S. J., 2009, *Icarus*, **202**, 160
- Devogèle M., et al., 2019, *AJ*, **158**, 196
- Galache J. L., Beeson C. L., McLeod K. K., Elvis M., 2015, *Planet. Space Sci.*, **111**, 155
- Granvik M., Morbidelli A., Vokrouhlický D., Bottke W. F., Nesvorný D., Jedicke R., 2017, *A&A*, **598**, A52

- Hinkle M. L., et al., 2015, in 46th Annual Lunar and Planetary Science Conference. Lunar and Planetary Science Conference. p. 1029
- Holmberg J., Flynn C., Portinari L., 2006, *MNRAS*, **367**, 449
- Hromakina T., et al., 2021, *A&A*, **656**, A89
- Ieva S., et al., 2018, *A&A*, **615**, A127
- Ieva S., et al., 2020, *A&A*, **644**, A23
- Kostov A., Bonev T., 2018, *Bulgarian Astronomical Journal*, **28**, 3
- Lin C.-H., Ip W.-H., Lin Z.-Y., Cheng Y.-C., Lin H.-W., Chang C.-K., 2018, *Planet. Space Sci.*, **152**, 116
- Mainzer A. K., Bauer J. M., Cutri R. M., Grav T., Kramer E. A., Masiero J. R., Sonnett S., Wright E. L., 2019, *NASA Planetary Data System*,
- Marsset M., et al., 2022, *AJ*, **163**, 165
- Penttilä A., Shevchenko V. G., Wilkman O., Muinonen K., 2016, *Planet. Space Sci.*, **123**, 117
- Perna D., Barucci M. A., Fulchignoni M., 2013, *A&ARv*, **21**, 65
- Perna D., et al., 2016, *AJ*, **151**, 11
- Perna D., et al., 2018, *Planet. Space Sci.*, **157**, 82
- Popescu M., Birlan M., Nedelcu D. A., 2012, *A&A*, **544**, A130
- Popescu M., et al., 2019, *A&A*, **627**, A124
- Ryan E. L., Woodward C. E., 2010, *AJ*, **140**, 933
- Schröder S. E., Grynko Y., Pommerol A., Keller H. U., Thomas N., Roush T. L., 2014, *Icarus*, **239**, 201
- Tholen D. J., 1984, PhD thesis, University of Arizona, Tucson
- Warner B. D., Harris A. W., Pravec P., 2009, *Icarus*, **202**, 134
- Wisdom J., 1983, *Icarus*, **56**, 51

APPENDIX A: ORBITAL ELEMENTS OF THE OBSERVED OBJECTS

APPENDIX B: INDIVIDUAL REFLECTANCE SPECTRA OF THE TARGETS

This paper has been typeset from a $\text{\TeX}/\text{\LaTeX}$ file prepared by the author.

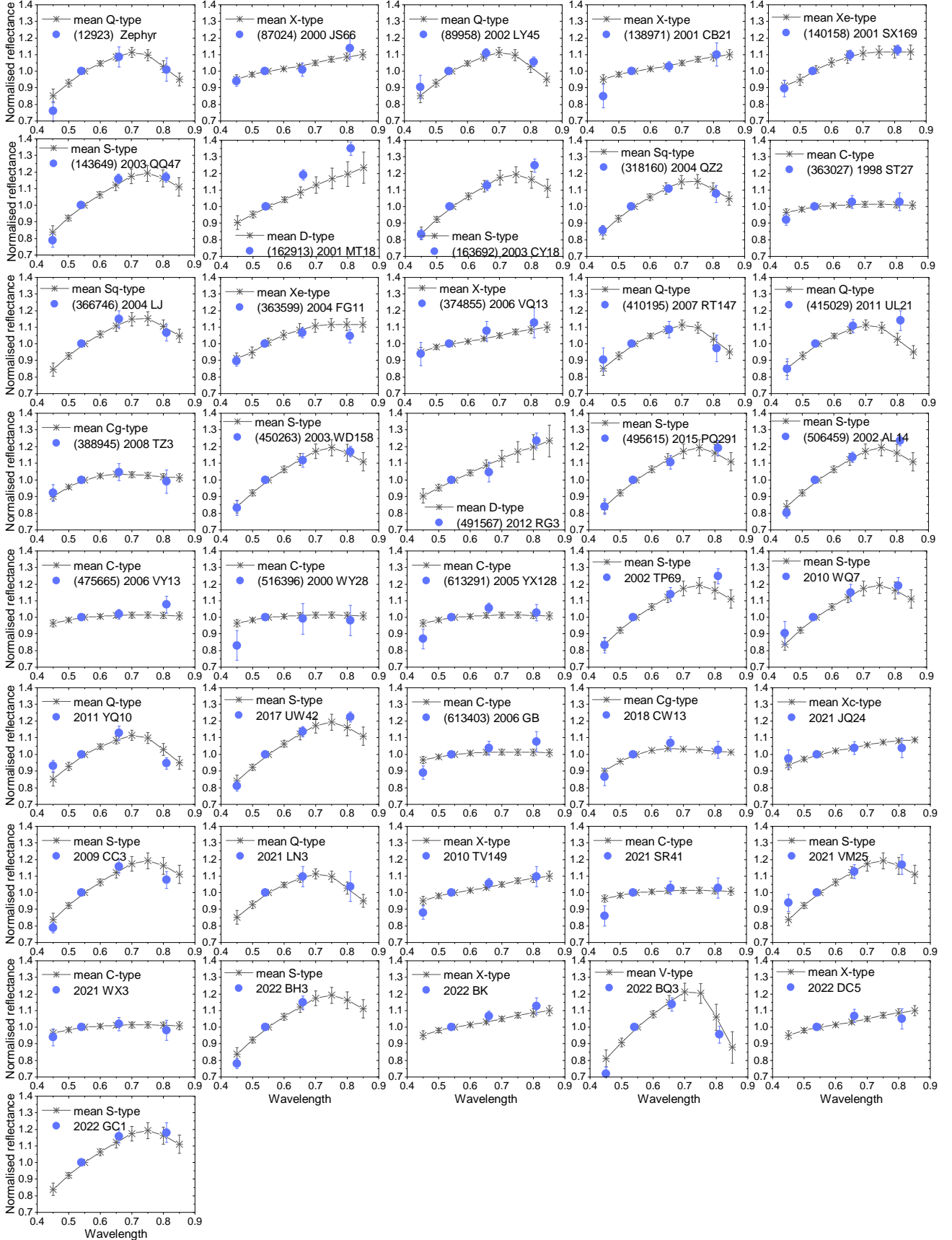


Figure B1. Individual reflectance spectra of the objects observed in this work (blue dots) together with the mean spectra of the most fitting taxonomic class from DeMeo et al. (2009) (black asterisks). The spectra are normalized at $0.54 \mu\text{m}$.

Table A1. List of observed objects and corresponding orbital elements taken from the MPC website.

	Object	Type	e	i, deg	a, au	q, au	Tj
1	(12923) Zephyr	Apollo, PHA	0.4922	5.305	1.9620	0.9962	3.716
2	(87024) 2000 JS66	Apollo	0.1899	14.431	1.1967	0.9694	5.260
3	(89958) 2002 LY45	Apollo, PHA	0.8862	9.908	1.6417	0.1867	3.682
4	(138971) 2001 CB21	Apollo, PHA	0.3333	7.899	1.0343	0.6895	5.863
5	(140158) 2001 SX169	Apollo, PHA	0.4609	2.518	1.3472	0.7262	4.764
6	(143649) 2003 QQ47	Apollo, PHA	0.1870	62.102	1.0850	0.8820	5.214
7	(162913) 2001 MT18	Apollo	0.5196	8.647	1.2709	0.6105	4.929
8	(163692) 2003 CY18	Apollo	0.4106	7.199	1.5266	0.8998	4.389
9	(318160) 2004 QZ2	Amor	0.4929	0.9691	2.261	1.1465	3.448
9	(363027) 1998 ST27	Aten, PHA	0.5300	21.062	0.8190	0.3850	6.978
10	(363599) 2004 FG11	Apollo, PHA	0.7238	3.1269	1.5872	0.4384	4.039
12	(366746) 2004 LJ	Apollo, PHA	0.4616	18.282	1.0865	0.5850	5.559
13	(388945) 2008 TZ3	Apollo, PHA	0.3907	8.7176	1.5900	0.9689	4.278
14	(374855) 2006 VQ13	Apollo, PHA	0.4457	16.698	1.0993	0.6093	5.521
15	(410195) 2007 RT147	Amor	0.4668	3.831	2.2912	1.2216	3.442
16	(415029) 2011 UL21	Apollo, PHA	0.6528	34.851	2.1228	0.7369	3.245
17	(450263) 2003 WD158	Apollo, PHA	0.4091	16.726	1.4264	0.8428	4.563
18	(475665) 2006 VY13	Amor	0.6137	4.673	4.6727	4.6727	2.960
19	(491567) 2012 RG3	Apollo	0.5286	15.918	1.5744	0.7422	4.203
20	(495615) 2015 PQ291	Aten	0.2374	34.602	0.9825	0.7493	5.991
21	(506459) 2002 AL14	Apollo	0.1261	22.998	1.0376	0.9067	5.830
22	(516396) 2000 WY28	Amor	0.2894	19.447	1.6384	1.1642	4.189
23	(613291) 2005 YX128	Apollo	0.7347	4.476	2.1744	0.5767	3.267
24	(613403) 2006 GB	Aten, PHA	0.1793	10.061	0.9590	0.7871	6.257
25	2002 TP69	Amor	0.4695	1.974	1.9475	1.0331	3.751
26	2009 CC3	Amor, PHA	0.5373	11.372	2.2006	1.0182	3.440
27	2010 TV149	Apollo, PHA	0.5188	9.792	1.6989	9.7926	4.025
28	2010 WQ7	Amor	0.5567	13.610	2.3699	1.0504	3.285
29	2011 YQ10	Amor	0.5216	2.397	2.2418	1.0724	3.440
30	2017 UW42	Amor	0.4842	6.670	2.4560	1.2667	3.313
31	2018 CW13	Apollo	0.7051	28.918	1.6108	0.4750	3.921
32	2021 JQ24	Amor	0.6695	5.993	3.2256	1.0659	2.776
33	2021 LN3	Apollo	0.5662	28.80	2.2776	0.9881	3.241
34	2021 SR41	Apollo	0.6502	21.935	2.3796	0.8324	3.140
35	2021 VM25	Apollo	0.3913	9.162	1.6474	1.0028	4.181
36	2021 WX3	Amor	0.5144	7.853	2.1988	1.0677	3.471
37	2022 BH3	Apollo	0.5972	3.943	2.1629	0.8711	3.437
38	2022 BQ3	Amor	0.6027	15.088	2.8279	1.1237	2.976
39	2022 BK	Amor	0.5801	10.713	2.4666	1.0357	3.212
40	2022 DC5	Apollo	0.2061	3.925	1.0142	0.8052	2.976
41	2022 GC1	Apollo	0.4006	13.331	1.1695	0.7009	5.294
42	2022 GY2	Apollo, PHA	0.8647	6.199	2.1673	0.2933	3.049